High pressure, Magnetic and Structural Properties of Chromium Doped Barium Ferrite Synthesized via Co-precipitation Method

S. Vadivelan[1,*]
[1,*]*Department of physics, Anna University, Chennai-600025, Tamilnadu, India*
*Email:starvel30@gmail.com

Abstract

In this paper, it is proposed to synthesize chromium-doped barium ferrite ($BaCr_xFe_{12-x}O_{19}$) using co-precipitation technique at different ratios in order to increase the coercivity value, which in turn increases the magnetic storage capacity of the chromium-doped barium ferrite. This method was used to prepare different ratio (0–8%) of chromium-doped barium ferrite samples exposed to sintering process under the temperature 1150°C for 6 h because the base and doped materials are combined to form a new compound. The sintered compound is involved the XRD analysis and the obtained values are matched with the constant standards (a = b = 5.881 Å and c = 23.161 Å). Hence, the samples proved as hexagonal system. Using beam of X-rays, XPS spectra obtained and the binding energy of the sample is measured. From high-pressure electrical study, the electrical resistivity of a precipitated pure and chromium doped barium ferrite were measured over the pressure range of 0 to 9 GPa. The dielectric properties such as dielectric constant found to decreasing with increasing frequency while ac electrical conductivity is observed to be increasing with the increasing in frequency. The vibrating sample magnetometer measures the magnetic saturation, magnetic reminisce and coercivity of a sample. The magnetic saturation, magnetic remanence and coercivity values are found and tabulated.

Keywords: ***Magnetic remanence, Magnetic saturation, Coercivity, ferrite.***

1. Introduction

The newly are increased physical and structural properties of Chromium is situated in-group 6 and d-block position in periodic table and one of the good transition metal. The periodic table shows that how the chemical elements are related to each other. Chromium shares many chemical and physical properties with these two elements vanadium and manganese because it is located between them. It is a hard and brittle metal but reasonably flexible. Chromium is wonderful magnetic material and more corrosion resistance with high hardenability. The magnetic properties of chromium are even more obvious in alloys (1-3). An alloy is made by melting and mixing two or more metals.

The mixture has different properties from those of the individual metals. It combines slowly with oxygen in the air, but does not catch fire and burn unless it is in a powder form. It reacts with most acids to produce hydrogen gas. Trivalent chromium ion is a necessary nutrient in trace amounts in humans for insulin, sugar and lipid metabolism while the issue is debated. The intensification effect of forming stable metal carbides at the grain boundaries and the strong increase in corrosion resistance made chromium an important alloying material for steel (4-6). In metallurgy, cementation is the process by a metal which is covered with a fine coating of a second metal. Cementation is used to make very hard, strong alloys, such as those used in drilling tools and dies. Recently chromium doped with nano barium ferrite for improved their magnetic properties and it used in magnetic storage device. Now, chromium doped with ferrite is used for improving their magnetic storage applications. The most application of this material is in world such as recording materials, permanent magnet and magnetic stripe cards (7-10).

The packing density of nano barium ferrite material is greater because the size of the material is reduced greatly. The stability of the material is high due to high packing density. This type of ferrite has to produce much higher coercively levels. This is the reason, which makes the hard magnetic material, therefore manufacture the ferrite material in to good recording medium (11-13). Chromium doped nano barium ferrite formed in any size and shape using by sintering process, where by powdered form nano barium ferrite heated until it is combined to form the new structure without losing magnetic properties. The recording area depends upon the packing density.

This type of ferrite particle size is reduced as much as possible to increase the recording efficiency with recording area. From the magnetic characterization, the above statement proved with the help of VSM characterization. The focal aspire of this work is to make the grade increase the storage capacity of chromium doped nano barium ferrite by increasing the dopant ratio of chromium produced by co-precipitation technique (14-16). In this chapter, the chromium doped nano barium ferrite powder particles prepared by co-precipitation technique with structural, thermal, morphology and magnetic properties were studied.

2. Experiment

2.1. Materials

The co-precipitation method is used to prepare pure and chromium doped barium ferrite. Purifiedbarium nitrate (Ba $(NO_3)_2$), ferric nitrate (Fe $(NO_3)_3$), chromium nitrate (Cr $(NO_3)_2$), citric acid ($C_6H_8O_7$) and ammonium hydroxide (NH_4OH) are purchased from scientific material and technology.

2.2. Synthesis

The stoichiometric amounts of barium nitrate (Ba $(NO_3))_2$, ferric nitrate (Fe $(NO_3)_3$) and chromium nitrate ((Cr $(NO_3)_2$) are mixed in deionized water with ammonium hydroxide (NH_4OH) and citric acid ($C_6H_8O_7$). Citric acid is used to obtain the clear product. The synthesizing process totally controlled by ammonium hydroxide to produce various doping percentages of chromium nitrate by co-precipitation method. The precipitated materials are collected by filtration method and washed 3 times with distilled water. The final precipitate material is sent to drying process at 80°C for 6 hours. The dried material is ground to powder and allowed to undergo sintering process at 1150°C for 6 hours. Finally, the chromium doped barium ferrite composition ($BaCr_xFe_{12-x}O_{19}$) is obtained by this technique.

2.2. Measurements

Powder is used in X-ray diffractometer (Bruker D2 Phaser) with CuK_α radiation (λ = 1.541 Å) in the range of 10º-80º to identify the structure of the powder material. Thermogravimetry/differential thermal analysis is involved to study the thermal stability of the material using TGA/DTA apparatus (Netzsch STA 409) with the temperature range of 10–1200°C.The pure and doped barium ferrite formation is analyzed using FTIR Spectrophotometer apparatus (BRUKER ALPH). Using X-Ray Photoelectron Spectroscopy (XPS), the oxidation states of these samples are obtained with the source operating pass energy with 160ev. The electrical resistivity of Bismuth has been found under various oil pressures. The bismuth transitions at 25.5, 27 and 77 k bar are used for pressure calibration. VSM characterization is used to find the magnetic properties of these samples with an applied magnetic field of 21 kOe at room temperature.

3. Result and Analysis

3.1. Thermal studies (TGA/DTA)

TG/DTA is used to determine the characteristics of materials that exhibit either mass loss or gain due to decomposition and oxidation. From TG/DTA, the degradation mechanisms, reaction kinetics, determination of organic content and determination of inorganic (e.g. ash) content in a sample are analyzed [18-20].

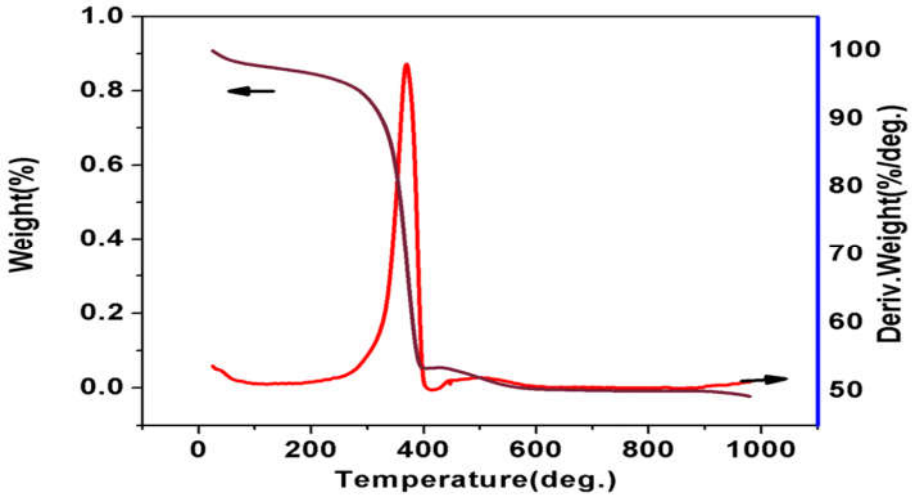

Fig.1. TG/DTA pattern for pure barium ferrite powder particles

The Fig. 1 shows the TG/DTA plots for the compound containing a mixture of $BaCo_3$, Fe_2O_3 and doping weight percentage of Cr $(NO_3)_2$is 2mol % respectively. The endothermic peak appeared in the DTA curvature on 840°C. From the diagram, it is clear that the decarboxylation of $BaCO_3$ represents the pure carbonate at 970°C and the mixture of carbonate with iron oxide takes, places around 778°C [21-22]. The complete structure of barium ferrite is indicated around 975-1150°C. The exothermic DTA curve indicates that residual of Co_3O_4 to Co_2O_3 transformation occurred at the temperature 575°C. The conversion of this reaction is very fast and it denoted by the manifestation of a sharp spear joined with the endothermic reaction [23-24]. Due to elasticity, the effect the hasty exothermic reaction it may be accurse.

3.2. Structural studies (XRD)

The XRD patterns for the synthesized pure and chromium doped barium ferritecompound shown in Fig. 2. The XRD characteristics confirm the crystal structure of pure barium ferrite is hexagonal according to JCPDS 78-0133. The strong diffraction peaks of pure barium ferrite samples exhibit standard peaks at 2θ values corresponding to (110), (107) and (114) planes respectively. The chromium doped barium ferrite structure is hexagonal according to JCPDS 52-1866. The strong diffraction peaks of chromium doped barium ferrite samples exhibit standard peaks at 2θ values corresponding to (114), (107) and (203) planes respectively [25].The absence of any other peaks (apart from $BaFe_{12}O_{19}$ peaks) in the XRD pattern indicates the purity of the synthesized samples. The broadening of the peaks indicates an increase from exterior to size fraction and decrease in the diameter of these particles. The crystalline sizes (t) of the prepared ferrite powder samples is determined by Scherrer formula [26],

$$t = \left(\frac{k\lambda}{\beta\cos\theta}\right) \qquad (1)$$

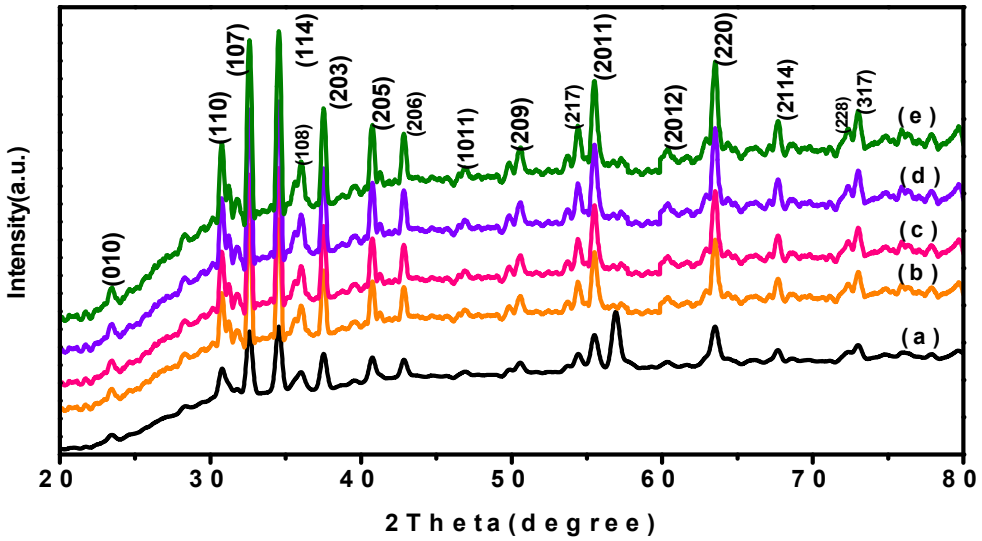

Fig.2. XRD pattern of the powder samples: (a) Pure barium ferrite and (b) Cr-2mol %, (c) Cr-4mol %, (d) Cr-6mol %, (e) Cr-8mol % doped barium ferrite powder particles.

where k denotes the Scherrer constant (k=0.9), λ is the well known wavelength of using X-ray source (λ=1.54 Å), β is the full width half maximum of the specified diffraction peak and θ is the diffracted angle of the powder samples [27-28]. The crystalline size (t) of the samples underneath study as quite different from single-line approach of the XRD reflections is tabulated (Table 1).

Table 1

samples	Crystalline size (nm)		Average crystalline size 't'(nm)	a (Å)	c (Å)	Elastic Strain ε (X 10^{-3})
	Scherrer method	W–H method				
Pure	33.6	36.7	35.15	5.869	23.103	3.98
Cr-2%	34.5	36.1	35.30	5.881	23.161	3.75
Cr-4%	36.3	36.7	36.50	5.869	23.103	3.81
Cr-6%	37.2	37.5	37.35	5.881	23.161	3.89
Cr-8%	37.9	38.7	38.30	5.869	23.103	3.92

From the data the crystalline size of pure barium ferrite is 35.15 nm, while doping Cr^{2+} in the barium of chromium ferrite increases the crystalline size. Thus, it can be concluded that the crystallite size strongly depends on Cr^{2+} concentration, which impedes the grain growth, thereby making the crystallite size to decrease with its increasing concentration. Table 1 shows the elastic strain whose value is increased with increasing Cr^{2+} concentration. It reveals that the possible growth of barium with chromium ferrite powder particles with larger defects in this favored direction; switches over to smaller crystallite size. The lattice constant "a" is calculated for all the compositions using this relation [29-30],

$$\frac{1}{d^2} = \frac{4}{3}\left[\frac{h^2+hk+k^2}{a^2}\right] + \frac{l^2}{c^2} \qquad (2)$$

"d" denotes the d spacing of the XRD pattern and h, k and l are the Miller indices. From the table, Cr^{2+} concentration increases the particle size also increased. The elastic strains of the samples also calculated by the given expression [31-32],

$$\varepsilon = \frac{\beta}{2\cot(\theta)} \qquad (3)$$

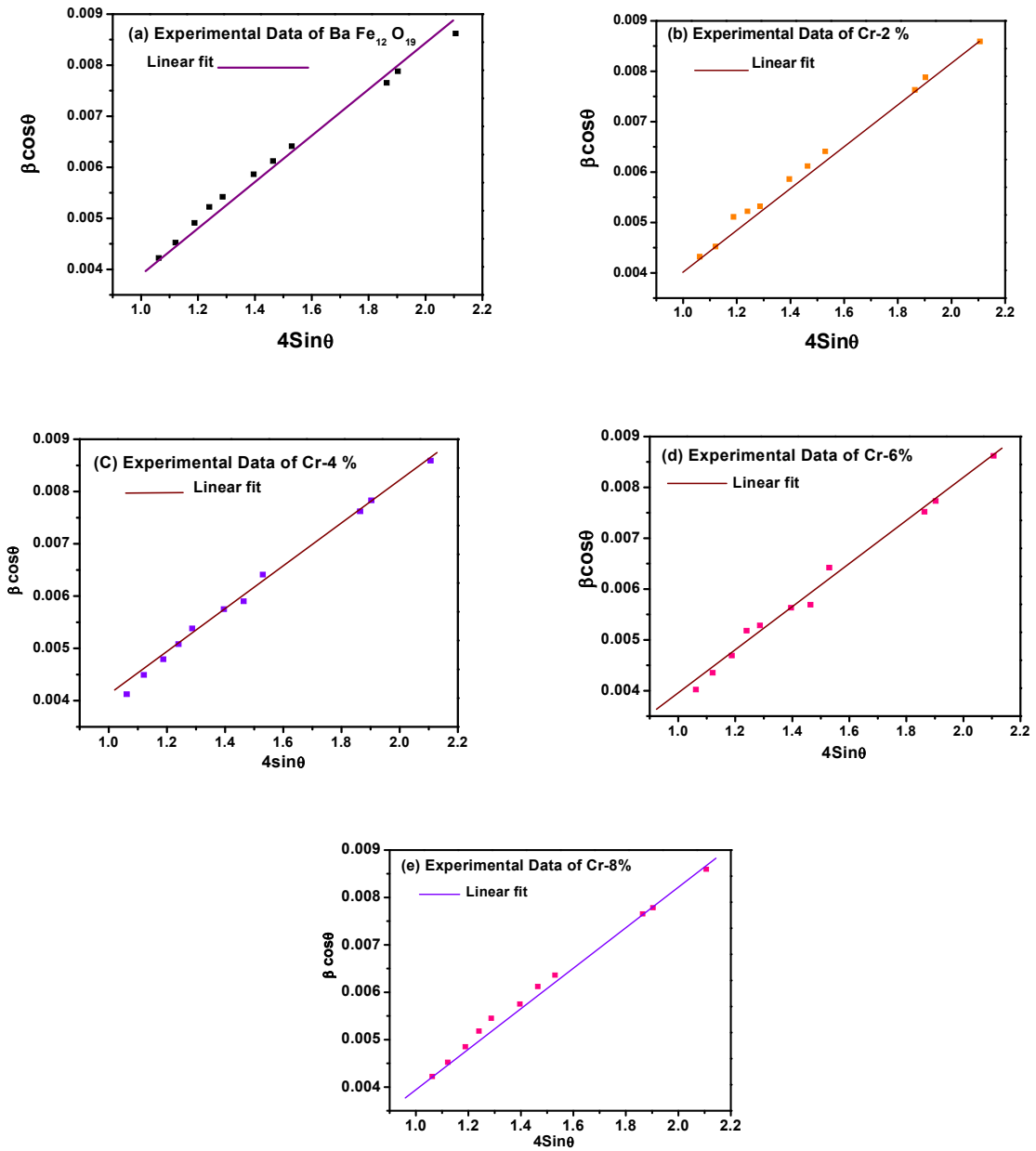

Fig.3. Williamson–Hall plot of the powder samples:(a) Pure barium ferrite, (b) Cr-2mol %, (c) Cr-4mol %, (d) Cr-6mol % and (e) Cr-8mol % doped barium ferrite powder particles

The elastic constant values are indexed in Table 1.The Cr^{2+} concentration is found to be increasing with a decrease in elastic constant of the powder samples. Using the Williamson and Hall method, the crystalline size of the powder samples is found [33-34].

$$\beta_{(hkl)}Cos\theta_{(hkl)} = \frac{K\lambda}{D} + 4\varepsilon Sin\theta_{(hkl)} \qquad (4)$$

K is known as the constant (0.9), λ is the wavelength of the X-ray source (1.5406 Å), D is the crystalline size, β be the full width half maximum of the specified diffracted peak, h, k, and l is the miller indices and ε is the micro strain. Using the above relation, the Williamson and Hall plot are drawn and slope line corresponds to strain as shown in Fig. 3.

3.3. Fourier Transforms Infrared Spectroscopy Studies (FT-IR)

FTIR spectrum investigation is used to find the information as regards bonding in a compound. The spectrum peaks are mainly dependent on the structure of the crystal, morphology and chemical mixing ratio of the prepared powder materials to determine the chemical bonding pure and Cr doped $BaFe_{12}O_{19}$ compounds. The FT-IR spectra of pure and Cr doped barium ferriteare recorded in the range of 500–3800 cm^{-1} wave numbers as shown in Fig. 4. The deep fascination bands Cr–O and Fe–O are present between the frequency ranges of 550–900 cm^{-1}. In addition, the fascination band below 450 cm^{-1} is due to the deformation of Fe–O bonds in the deformation of Fe–O–Fe bridges [35-36]. The intense fascination peak around 769 $cm^{-1}$is related with O–Fe–O vibration mode. Moreover, the OH stretching vibration and water molecules are present in the range respectively 3100-3350 cm^{-1} and 1498 cm^{-1}.

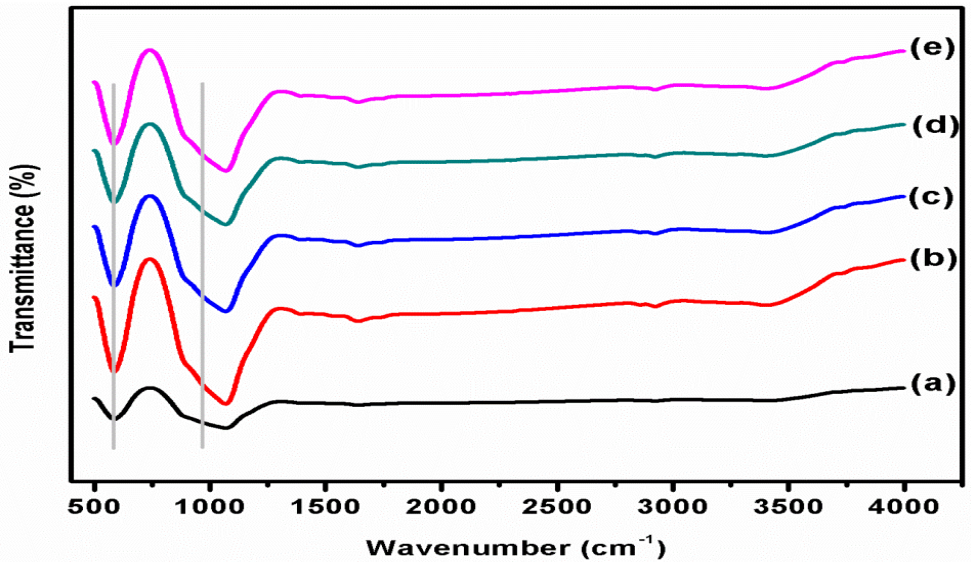

Fig.4. FT-IR pattern of the powder samples: (a) Pure barium ferrite, (b) Cr-2mol %, (c) Cr-4mol %, (d) Cr-6mol % and (e) Cr-8mol % doped barium ferrite powder particles

The bending mode of H–O–H is also located at the same range of water molecules [37-39]. Increase in doped concentration of chromium nitrate, the O-C-O stretching band is present in the range 2215 cm^{-1} [40-41]. The material segment and chemical spotlessness of pure and Cr doped barium ferritecompounds are present in the spectra range of 400–4000 cm^{-1}.

3.4. X-Ray Photoelectron Spectroscopy Studies (XPS)

Fig. 5 shows the XPS spectra of the Crdoped barium ferrite material synthesized by co-precipitation method. The X-Ray photoelectron spectroscopy (XPS) is used to analyze the plane and chemical states of the synthesized samples. The peaks of spectrum of C 1s, O 1s, Fe 2p and Cr 2p are observed in this

spectrum [42-44]. The fig. 6a shows that, the Ba 3*d*3/2 and Ba 3*d*1/2 peaks observed at 780.8ev and 784.6ev respectively, which are used to characterize the sample. Ba^{2+} ion is presented in the compounds and it represents the binding energy spectrum. Fig. 6b shows the presence of XPS spectra of Cr doped barium ferrite peaks Cr 2p1/2 and Cr 2p3/2 at the obligatory power values of 893.4 eV and 889.5 eV. These peaksconformed the Cr^{2+} ion present in the barium ferrites [45-47]. Fig. 6c shows the Fe 2p center crust XPS spectra of chromium ferrite. This result is in close agreementwith previous literature for Fe^{3+} ion in ferrite materials. Significantly, the high-resolution XPS spectra of Fe 2p shown in Fig. 6c can be fitted into two distinct peaks located at 708.73 eV and 713.43 eV.

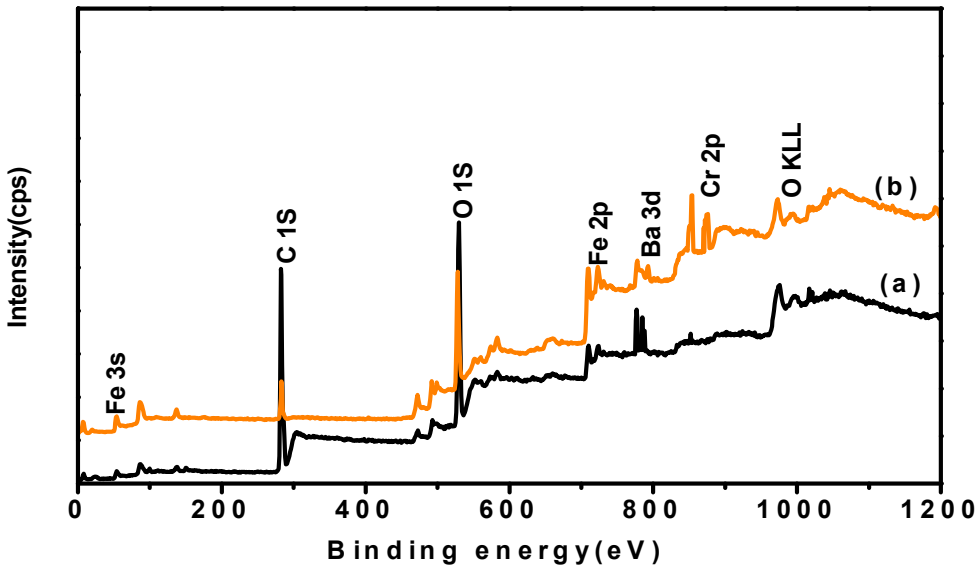

Fig.5. XPS spectrum: (a) pure barium ferrite powder particles and (b) Cr-2mol % doped barium ferrite powder particles

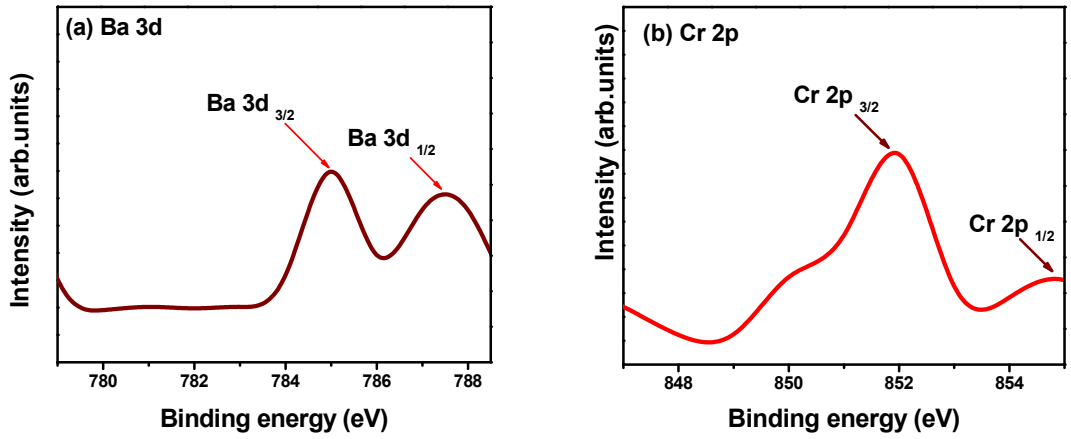

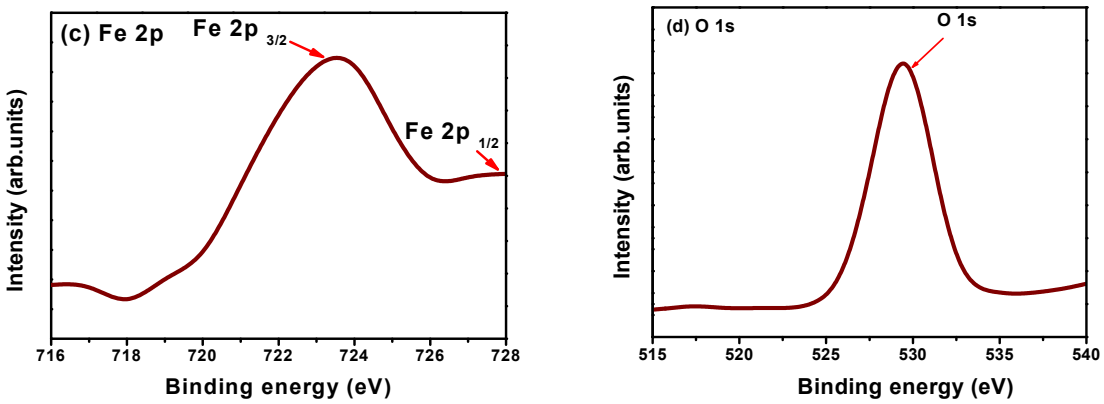

Fig.6. XPS high resolution spectrum: (a) Ba 3d, (b) Cr 2p, (c) Fe 2p and (d) O 1s

These peaks correspond to the obligatory power of Fe 2p3/2-Fe^{2+} and Fe 2p3/2-Fe^{3+} ions. Therefore, the oxidation states of iron (Fe) in the prepared nanoparticles definitely consist of both Fe^{3+} and Fe^{2+} ions [48]. From the XPS spectra of the O 1s region found at 534.23 eV, as shown in Fig. 6d. This peak is associated with corresponding binding energy of O^{2-} metal group observed from the surface of the sample.

3.5. High pressure electrical resistivity studies

The Fig. 7 shows relative resistivity changes with rising pressure for pure and Cr-doped barium ferrite. The pressure is increasing from 0 to 10 GPa, there is no possible to change the structure. This result is controversy to the previous result [49-50]. In this study, the electrical resistivity of a precipitated pure and chromium doped barium ferrite were measured over the pressure range of 0 to 9 GPa.

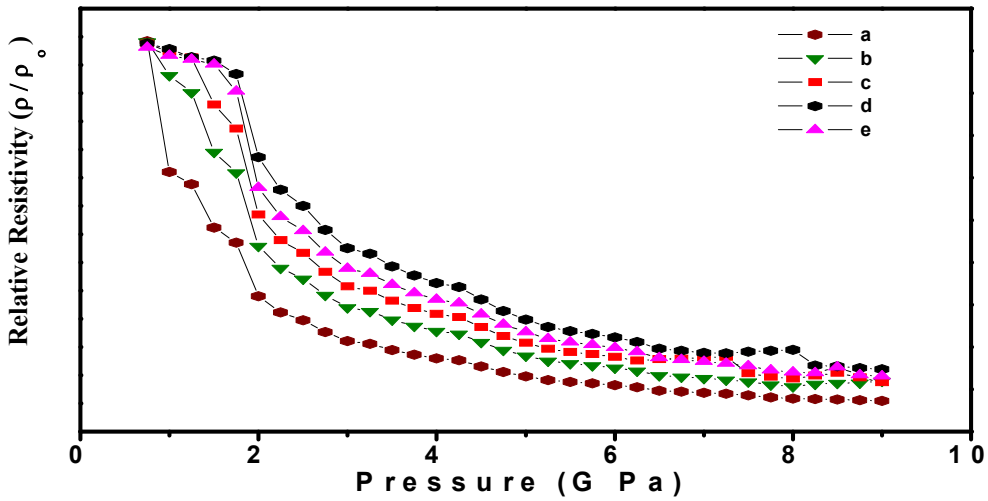

Figure 7 High Pressure induced electrical resistivity of the samples: (a) Pure barium ferrite and (b) Cr-2mol %,(c) Cr-4mol %, (d) Cr-6mol % (e) Cr-8mol % doped barium ferrite

However, the pressure is increasing up to 15 GPa there is no structure changes. This result well agrees with which means there is no any phase transition due to pressure induced internal volume change. It further confirms the presence of Cr in the barium matrix prevent the structural modification during under pressurization. This may be due to the presence of low ionic radius Cr in barium site could form the strong covalent bond with oxygen. The doping of Cr can provide the additional holes to conduction, which may reduce the electrical resistivity of the sample under compression. Otherwise, due to the high pressure the oxygen defects can be increases, which enhance the electrical conductivity significantly [51]. The systematic decrease of relative resistivity was observed with increase of pressure and chromium concentration. Fig. 7 shows at 8 mol% of Cr-doped barium ferrite shows rapid decrease in relative resistivity upto 1 GPa and further decreases almost linearly with increasing pressure to 9 GPa. It indicates that the high concentration of Cr could involve more electrons hole trapping process under high pressure.

3.6. Dielectric studies

Fig. 8 shows that dielectric constant with frequency in the range of 10 Hz to 1 MHz for pure and different dopant ratio of chromium. From results, the frequency is indirectly proportional to the dielectric constant. This results matches with the previous results [52-53]. The frequency increasing with decreasing dielectric constant can be explained based on applied ac field on axes direction. The electrons turn around the direction of motion much more frequently when the frequency of applied field is increased. Based on electronic polarization, the electrons reaching the grain boundary and thereby in the increasing frequency with decreasing dielectric constant. This material accredited to exhibit the good result for dielectric constant.

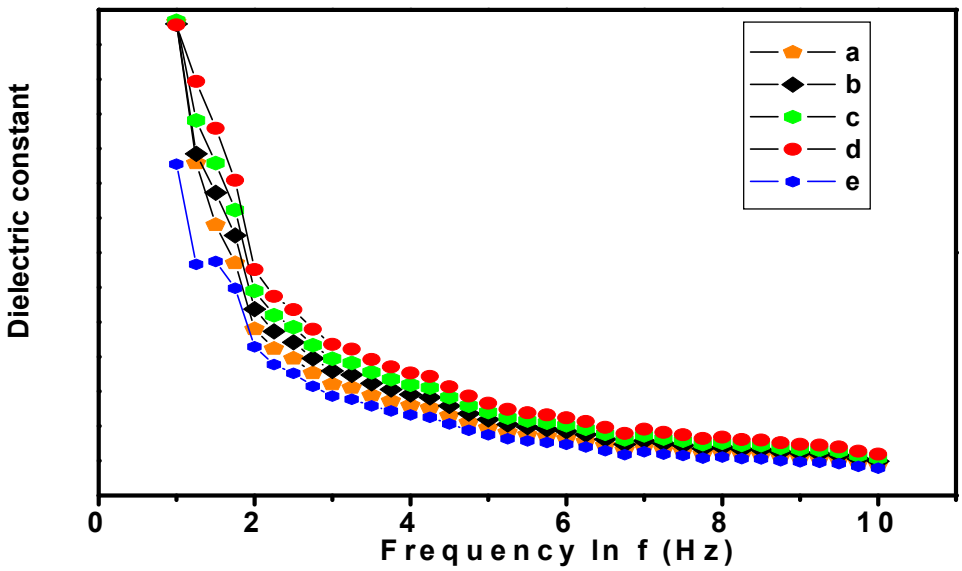

Figure 8 Dielectric constant with frequency images of the samples: (a) Pure barium ferrite and (b) Cr-2mol %,(c) Cr-4mol %, (d) Cr-6mol % (e) Cr-8mol % doped barium ferrite

3.7. Scanning Electron Microscope Studies (SEM)

From the scanning electron microscope analysis, the grain size and morphology of the prepared pure and chromiumdoped barium ferrite samples are found. The grain size increased with increasing the Cr doped percentage shown in fig.9.

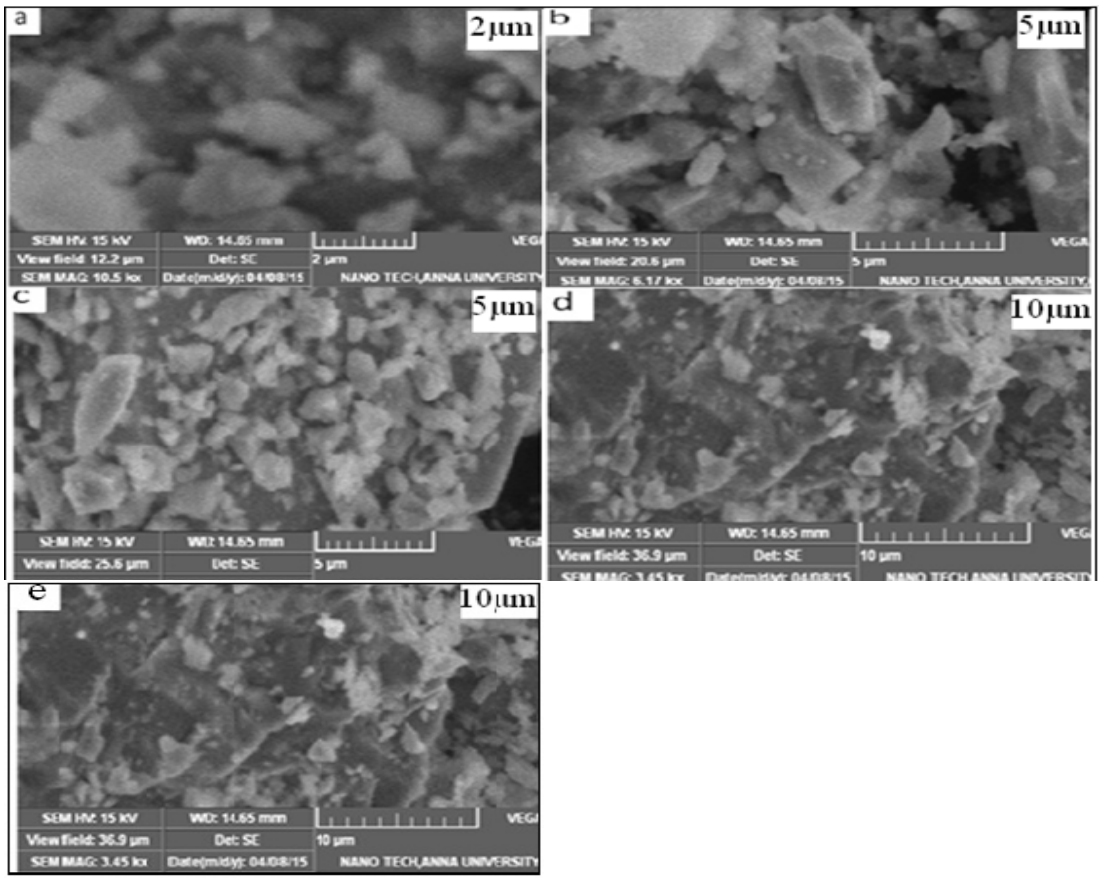

Fig.9. SEM image of the powder samples: (a) Pure barium ferrite and (b) Cr-2mol %, (c) Cr-4mol %, (d) Cr-6mol %, (e) Cr-8mol % doped barium ferrite.

From fig.9, the grain size increases in the order of 2-10µm with increasing chromium doped percentage (0-8%) [54-55]. Barium ferrite particles have comparatively a large air gap between each other, which reduces the strength of relations between separated particles. This characterization is mainly used to identify the material porosity of that material.

3.8. Magnetic studies

From the magnetic studies, the magnetic saturation, magnetic remanence and coercivity values are found [56-57]. The hysteresis loops for pure and chromiumdoped barium ferrite are shown in Fig. 10. The measurements of the magnetic data's are summarized in Table 2.After doping, the observed saturation magnetization (Ms) increasesfrom 11.7 to34.9 emu/g with increase in the chromium percentage.The saturation magnetization (Ms) value of pure barium ferrite is 11.7emu/g at 300K.

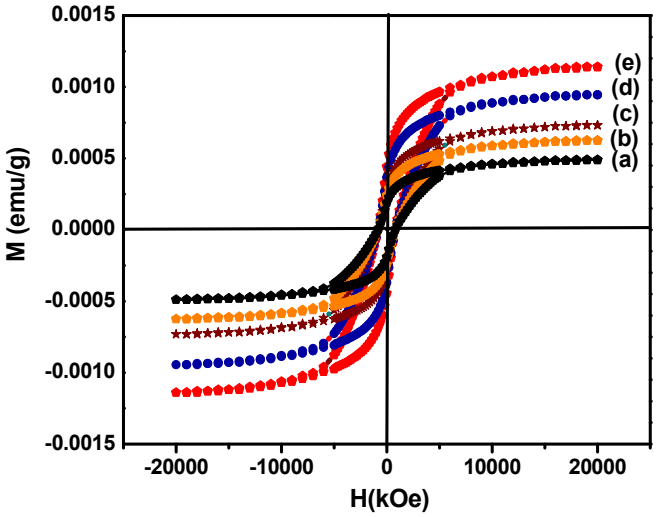

Fig.10. Hysteresis patterns for powder samples: (a) Pure barium ferrite and (b) Cr-2mol %, (c) Cr-4mol %, (d) Cr-6mol %, (e) Cr-8mol % doped barium ferrite.

From the hysteresis loop, the remnant magnetization (Mr) of the pure and chromiumdoped barium ferrite is increased with increase in doped percentage of chromium [58]. The remnant magnetization (Mr) at 300K for pure and chromiumdoped barium ferrite is 4.09 emu/g and 9.13-25.9 emu /g. From this ratio (Mr/Ms), the squareness values are obtained. The SQR value increases with increasing doped percentage of chromium [59-60]. The SQR value of the pure barium ferritesamples at 300 K is 0.349 and doped percentage of chromiumis increased thereby increasing the SQR value simultaneously.

Table 2

Sample	**Ms (Saturation magnetization) (emu/g)**	**Mr (Remnant magnetization) (emu/g)**	**(Mr/Ms) ratio**	**Hc (Coercivity) (Oe)**
Pure	11.7	4.09	0.349	851.128
Cr-2%	25.4	9.13	0.359	853.168
Cr-4%	28.7	10.89	0.379	857.179
Cr-6%	33.9	13.17	0.388	860.789
Cr-8%	35.3	25.9	0.733	862.665

From the hysteresis loop, the SQR value of 8% chromium doped barium ferrite is calculated as 0.733 at 300 K. However, the SQR values depend on the temperature.The coercivity value for pure barium ferrite is 851.128 Oe at 300K. In addition, the chromium-doped percentage (0-8%) is increased with increasing the coercivity value (851.128-862.665 Oe). After doping, the observed Ms Value increases from 25.4 emu/g to 35.3 emu/g with increase in the chromiumdoped percentage. From the data, SQR value is obtained as dependency of the temperature and chromiumdoped percentage. Based on the sample density, SQR and coercivity value is varied.

4. Conclusion

Hexagonal structure chromium doped barium ferrite was effectively synthesized via co-precipitation technique. From the XRD analysis established, the configuration of pure barium is hexagonal structure and chromium doped barium ferrite is hexagonal structure. High-pressure electrical resistivity can explained no other structural changes during under pressurization. The frequency increasing with decreasing dielectric constant explained clearly based on applied ac field on axes direction. The SEM image clearly explained that with the dopant ratio's increase simultaneously grain size also increased from 2μm to 10μm respectively. Hysteresis loop results show the coercivity (Hc) increased sharply from 851.128 - 856.321 Oe for increasing the dopant ratios of chromium at 300K.The main aim of this work is to increase the storage capacity of this material because we avoid the more number of storage capacitor due to convenience. The magnetic properties of these samples are affected greatly through the preparation and sintering process. This method is very easy, low cost and preparation area is companionable. Based on results and experimental method this technique is remarkable compared to other techniques.

Acknowledgments

The authors thankfully acknowledge research support from the Anna University and IITM, Tamilnadu, India.

References

[1] *Sozeri, H. Kucuk, L. Ozkan, H. Improvement in magnetic properties of La substituted $BaFe_{12}O_{19}$ particles prepared with an unusually low Fe/Ba molar ratio, Journal of Magnetism and Magnetic Materials 323 (2011) 1799-1804.*

[2] *Salvi, S.V. Joshi, V.H. Effect of PH on magnetic properties of doped barium hexaferrite, Indian Journal of Pure & Applied Physics 4 (2009) 277-281.*

[3] *Gubin, S.P. Koksharov Yu, A. Khomutov, G.B. YurkovYu,G. Magnetic nanoparticles: preparation, structure and properties, Russian Chemical review 74 (2005) 489-520.*

[4] *Murthy, Y.L.N. Kasiviswanath, I.V. Synthesis and characterization of nickel copper ferrite, International Journal of ChemTech Research 1 (2009) 1308-1314.*

[5] *Hessien, M. Rash ad, M. El-Barawy, K. Controlling the composition and magnetic properties of strontium hexaferrite synthesized by co-precipitation method, J. Magn. Magn. Mater. 320 (2008) 336–343.*

[6] *Schloemann, E. Advances in ferrite microwave materials and devices, J. Magn. Magn. Mater. 209 (2000) 15-20.*

[7] *Altenburg, H. Plewa, J. Plesch, G. Shpotyuk, O. Influence of the agglomeration in the initial suspension (ferrofluid) on the oriented magnetic structure, Pure Appl. Chem. 74 (2002) 2085-2093.*

[8] *Biest, O. VandeperreAnnu, L. Electrophoretic deposition of materials, Rev. Mater. Sci. 29 (1999) 327-352.*

[9] *Carp, O. Barjega, R. Segal, E. Brezeanu, M. Nonco-nventional methods for obtaining hexaferrites,ThermochimicaActa, 318 (1998) 57-63.*

[10] *Garcia-Casillas, P.E. Beesley, A.M. Bueno, D. Martinez, C.A. Remanence properties of barium hexaferrite, Journal of Alloys and Compounds 369 (2004) 185-196.*

[11] *Makled, M.H. Matsui, T. Tsuda, H. Mabuchi, H. El- Mansy, M.K. Infrared Spectroscopy and Thermal Stability Studies of Natural Rubber-Barium Ferrite Composites, Journal of Materials Processing Technology 160 (2005) 229-233.*

[12] *Golosovsky, M. Saado, Y. Davidov, D. Self-assembly of floating magnetic particles into ordered structures: A promising route for the fabrication of tunable photonic band gap materials, Applied Physics Letters 7 (1999) 4168-4175.*

[13] *Hur, N.H. Park, J.Y. Dho, Kim, S.J. Lee, E.K. Magnetic and microstructural properties on Mn- and Ru-doped hexagonal barium ferrites, IEEE Trans. Magn. 40 (2004) 2790–2792.*

[14] *Singh,P. Babbar, V.k. Razdan, A. Srivastava, S.L. Agrawal, V.K. Goel, T.C. Dielectric constant, magnetic permeability and microwave absorption studies of hot-pressed Ba-Co Ti hexaferrite composites in X-band, J. Mater. Sci. 41 (2006) 7190–7196.*

[15] *Shams, N. Liu, X. Matsumoto, M. Morisako, A. Microstructure and magnetic properties of commercial barium ferrite powders, Journal of Magnetism and Magnetic Materials 290 (2005) 138-140.*

[16] *Dobrzaski, L.A. Drak, M. Zibowicz, B.Materials with specific magnetic properties, Journal of Achievements in Materials and Manufacturing Engineering 17 (2006) 37-43.*

[17] *Zibowicz, B. Szewieczek, D. Dobrzaski, L.A. New possibilities of application of composite materials with soft magnetic properties, Journal of Achievements in Materials and Manufacturing Engineering 20 (2007) 207-217.*

[18] *Qiu, J. Gu, M.Magnetic nanocomposite thin films of $BaFe_{12}O_{19}$ and TiO_2 prepared by sol–gel method, Applied Surface Science 252 (2005) 888-892.*

[19] *Mali, A. Ataie, A.Structural characterization of nano-crystalline $BaFe_{12}O_{19}$ powders synthesized by sol–gel combustion route, ScriptaMaterialia 53 (2005) 1065-1070.*

[20] *Drak, M. Dobrzaski, L.A.Corrosion of Nd-Fe-B permanent magnets, Journal of Achievements in Materials and Manufacturing Engineering 20 (2007) 239-242.*

[21] *Ding, J. Miao, W.F. McCormick, P.G. Street, R. High-coercivity ferrite magnets prepared by mechanical alloying, Journal of Alloys and Compounds 281 (1998) 32-36.*

[22] *Temuujin, J. Aoyama, M. Senna, M. Masuko, T. Ando, C. Kishi, H. Synthesis of Y-type hexaferrites via a soft mechanochemical route, J. Solid State Chem. 177 (2004) 3903-3908.*

[23] *Vadivelan, S. Victorjaya, N. Investigation of Structural, Thermal and Magnetic properties of Strontium substituted Barium Hexaferrite Synthesized via co-precipitation Method, International Journal of ChemTech Research 8 (2015) 404-410.*

[24] *Prasad, N.K. Naulakha, A. Jha, N. Meena, S.S. Bahadur, D. Prakash, O. Mandal, R.K.Magnetic and electric properties of nanoparticles of Ni-substituted ferrites synthesized using a microwave refluxing process, Int. J.Mater.Res.104 (2012) 680-685.*

[25] *Singhal, S. A comparative study on the magnetic properties of $MFe_{12}O_{19}$ and $MA_lFe_{11}O_{19}$ (MQSr, Ba and Pb) hexaferrites with different morphologies, Ceram. Int. 37 (2011) 1833–1837.*

[26] *Q. Xing, Q. Peng, Z. Wanga, C.B. Fu Z. Fu, X. Structural, electrical and dielectric properties of yttrium substituted nickel ferrites, Physica B407 (2012) 388-395.*

[27] *Ishaque, M. Islam, M.U. Azhar Khan, M. Rahman, I.Z. Genson A. Hampshire, S. Microstructure and Microwave Absorption Properties of Y-Substituted Ni-Zn Ferrites, Physica B. 405 (2010) 1532-1540.*

[28] *Haralkar, S.J. Kadam, R.K. More, S.S. SagarE.Shirsath, Mane, M.L. SwatiPatil Mane, D.R. Substitution effect of Cr3þ ions on the properties of Mg–Zn ferrite nanoparticles, Physica B 407 (2012) 4338–4346.*

[29] *Tholkappiyan, R. Vishista, K. N-N-methylene bis acrylamide: A novel fuel for combustion synthesis of zinc ferrite nanoparticles and studied by X-Ray photoelectron spectroscopy, International Journal of ChemTech Research6 (2014) 2834-2842.*

[30] *Nowosielski, R. Babilas, R. Dercz, G. Pajqk L. Wrona, J. Barium ferrite prepared by milling and annealing, Archives of materials science and engineering 22 (2007) 45-48.*

[31] *Drofenik, M. The hydrothermal synthesis of super-paramagnetic barium hexaferrite particles, Mater.Chem.Phys.127 (2011) 415–419.*

[32] *Patange, S.M. Shirsath, S.E. Toksha, B.G. Jadhav S.S. Jadhav, K.M. Electrical and magnetic properties of Cr3þ substituted nanocrystalline nickel ferrite, Journal of Applied Physics 106 (2009) 023914.*

[33] *Asghar, G. Anis-ur-Rehman, M. Structural, dielectric and magnetic properties of Cr–Zn doped strontium hexa-ferrites for high frequency applications, J. Alloys Compound 526 (2012) 85-90.*

[34] *Iqbal, M.J. Ashiq, M.N. Physical and electrical properties of Zr–Cu substituted strontium hexaferrite nanoparticles synthesized by co precipitation method, Chem. Eng. J. 136 (2008) 383.*

[35] *Kajal K MallickMagnetic properties of cobalt substituted M-type barium hexaferrite prepared by co precipitation, Journal of Magnetism and Magnetic Materials312 (2007) 418-429.*

[36] *Khademi, F. Structural, magnetic and microwave properties ofEu-doped barium hexaferrite powders, J. Supercond. Novel Magn. 25 (2012) 525–531.*

[37] *Hakola, A. Heczko, O. Jaakkola, A. Kajava, T. Ullakko, K. Pulsed laser deposition of NiMnGa thin films on silicon, Applied physics A 79 (2004) 1505-1508.*

[38] *Zhang, J.M. Zhang, Y. Xu, K.W. Ji, V. General Compliance Transformation Relation and Applications for Anisotropic Hexagonal, Metals Solid State Communications139 (2006) 87-91.*

[39] *Pramanik, N.C. Fujii, T. Nakanishi, M. Takada, J. Seok, S.I. The effect of heat treatment temperature on the microstructure and magnetic properties of $Ba_2Co_2Fe_{12}O_{22}$ (Co_2Y) prepared by sol–gel method, MaterLett. 60 (2006) 2718-2722.*

[40] *Yogamalar, R. Srinivasan, R. Vinu, A. Ariga, K. Bose, A.C. X ray peak broadening analysis in ZnO nanoparticles, Solid State Commun. 149 (2009) 1919-1923.*

[41] *Zhong, W. Ding, W. Zhang, N. Hong, J. Yan, O. Du, Y. Key step in synthesis of ultrafine $BaFe_{12}O_{19}$ by sol-gel technique,J. Magn Mater 168 (1997) 196-202.*

[42] *Jun Li Zhang Structural and Magnetic Behavior of Cobalt Doped $Ba_{0.5}Sr_{0.5}Fe_{12}O_{19}$ Nanoparticles Synthesized by Chemical Co-Precipitation Technique, Applied Mechanics and Materials 274 (2013) 406-410.*

[43] *Kim, S.G. Wang, W.N. Iwaki, T. Yabuki, A. Okuyama, K. Low-temperature crystallization of barium ferrite nanoparticles by a sodium citrate-aided synthetic process, J. Phys. Chem.C111 (2007) 10175–10180.*

[44] *Maensiri,S. Masingboon, C. Banjong, C. Seraphin, S. A simple route to synthesize nickel ferrite ($NiFe_2O_4$) nanoparticles using egg white, Scr. Mater. 56 (2007) 797–800.*

[45] *Nowosielski, R. Babilas, R. Dercz, G. Pajak, L. Microstructure of composite material with powders of barium ferrite, Journal of Achievements in Materials and Manufacturing Engineering 17 (2006) 117-120.*

[46] *Shepherd, P. Mallick, K. Green, R. Magnetic and structural properties of M-type barium hexaferrite prepared by coprecipitation, Journal of Magnetism and Magnetic Materials 311 (2007) 683–692.*

[47] *Mosleh, Z. Kamelin, P. Ranjbar, M. Salamati, H. Effect of annealing temperature on structural and magnetic properties of $BaFe_{12}O_{19}$hexaferrite nanoparticles, Ceramics International 40 (2014) 7279–7284.*

[48] *Jotania, B. Patel, A. Microstructure and Dielectric Properties of Mn Substituted $Sr_2Cu_2Fe_{12}O_{22}$ (Cu_2Y) Hexaferrite Powder, IJERA 2 (2012) 494-498.*

[49] *Zhao, Precursor-directed synthesis of quasi-spherical barium ferrite particles with good dispersion and magnetic properties, CrystEng Comm. 15 (2013) 808–815.*

[50] *Ravinder, D. Characterization of Co1-XZnxFe2o4 Nano Spinal Ferrites Prepared by Citrate Precursor Method, Int. Journal of Engineering Research and Applications 3 (2013) 654-660.*

[51] *Shobana, M.K. Calcium doped nickel ferrit powders prepared by sol-gel combustion method, International Journal of NanoDimension2 (2012) 275-279.*

[52] *Sharma, P. Rocha, R.A. De Medeiros, S.N. PaesanoJr, A. Structural and magnetic studies on barium hexaferrites prepared by mechanical alloying and conventional route, J. Alloys Comp 443 (2007) 37–42.*

[53] *TalwinderKaur, Srivastava, a.k. Effect of pH on Magnetic Properties of Doped Barium Hexaferrite, JRMET 3 (2013) 171-173.*

[54] *Lechevallier, L. Le Breton, J.M. Wang, J.F. Harris, I.R. Structural analysis of hydrothermally synthesized $Sr_{1-x}Sm_xFe_{12}O_{19}$ hexagonal ferrites, J. Magn. Magn.Mater. 269 (2004)192-196.*

[55] *Pullar, R.C Hexagonal ferrites: a review of the synthesis, properties and applications of hexaferrite ceramics, Prog. Mater. Sci. 57 (2012) 1191–1334.*

[56] *Shams, N. Liu, X. Matsumoto, M. Morisako, A. Microstructure and magnetic properties of commercial barium nanoferrite powders, Journal of Magnetism and Magnetic Materials, 290 (2005)138-140.*

[57] *Temuujin, J. Aoyama, M. Senna, M. Masuko, T. Ando, C. Kishi, H. Synthesis of Y-type hexaferrites via a soft mechanochemical route, J. Solid State Chem., 177 (2004) 3903-3908.*

[58] *Vadivelan, S. Victorjaya, N. Investigation of Structural, Thermal and Magnetic properties of Strontium substituted Barium Hexaferrite Synthesized via co-precipitation Method, International Journal of ChemTech Research, 8 (2015) 404-410.*

[59] *Asghar, G. Anis-ur-Rehman, M. Structural, dielectric and magnetic properties of Cr–Zn doped strontium hexa-ferrites for high frequency applications, J. Alloys Compound, 526 (2012) 85-90.*

[60] *Drofenik, M. The hydrothermal synthesis of super-paramagnetic barium hexaferrite particles, Mater.Chem.Phys., 127 (2011) 415–419.*